Supporting Information

Liu et al. 10.1073/pnas.1715477115

SI Notes

Carriers' Interactions and Transport Properties. To extract the thermoelectric transport properties from the Boltzmann transport equation (BTE), we need to understand the lifetime of carriers upon their interactions. According to Fermi's golden rule and under the relaxation time approximation (RTA), the scattering rates of electron and phonon due to the *e*-ph interactions are given by (1)

$$\frac{1}{\tau_{n\mathbf{k}}^{e\text{-ph}}}=\frac{2\pi}{\hbar}\sum_{m,p}\int\frac{d\mathbf{q}}{\Omega_{\mathrm{BZ}}}\left|\mathbf{M}_{n\mathbf{k},p\mathbf{q}}^{m\mathbf{k}+\mathbf{q}}\right|^2\left[\begin{array}{c}\left(f_{m\mathbf{k}+\mathbf{q}}+n_{p\mathbf{q}}\right)\delta\left(\varepsilon_{n\mathbf{k}}-\varepsilon_{m\mathbf{k}+\mathbf{q}}+\hbar\omega_{p\mathbf{q}}\right)\\+\left(1-f_{m\mathbf{k}+\mathbf{q}}+n_{p\mathbf{q}}\right)\delta\left(\varepsilon_{n\mathbf{k}}-\varepsilon_{m\mathbf{k}+\mathbf{q}}-\hbar\omega_{p\mathbf{q}}\right)\end{array}\right] \quad \textbf{[S1]}$$

and

$$\frac{1}{\tau_{p\mathbf{q}}^{\text{ph-}e}}=\frac{2\pi g_e}{\hbar}\sum_{m,n}\int\frac{d\mathbf{k}}{\Omega_{\mathrm{BZ}}}\left|\mathbf{M}_{n\mathbf{k},p\mathbf{q}}^{m\mathbf{k}+\mathbf{q}}\right|^2\left[\left(f_{n\mathbf{k}}-f_{m\mathbf{k}+\mathbf{q}}\right)\delta\left(\hbar\omega_{p\mathbf{q}}+\varepsilon_{n\mathbf{k}}-\varepsilon_{m\mathbf{k}+\mathbf{q}}\right)\right], \quad \textbf{[S2]}$$

respectively, where $\mathbf{M}_{n\mathbf{k},p\mathbf{q}}^{m\mathbf{k}+\mathbf{q}}$ is the coupling matrix of one *e*-ph scattering process, which informs the transition of an electron from band n and wave vector $\mathbf{k}$ to band m and wave vector $\mathbf{k}+\mathbf{q}$ participated by a phonon with mode p and wave vector $\mathbf{q}$. The amplitude of the coupling matrix indicates how strong the scattering channel of a given material is. $\varepsilon_{n\mathbf{k}}$ and $f_{n\mathbf{k}}$ are electron energy and Fermi–Dirac occupation, and $\omega_{p\mathbf{q}}$ and $n_{p\mathbf{q}}$ are phonon frequency and Bose–Einstein occupation. g_e is the degeneracy of the electron. The first term in the brackets in Eq. **S1** corresponds to the phonon-absorption process, and the second term corresponds to the phonon-emission process. The coupling matrix is the key in studying such transition problems. Technically we can treat the variation of crystal potential induced by collective atomic vibrations as a perturbation to the system, and thus the matrix element can be evaluated by (1)

$$\mathbf{M}_{n\mathbf{k},p\mathbf{q}}^{m\mathbf{k}+\mathbf{q}}=\left(\frac{\hbar}{2m_0\omega_{p\mathbf{q}}}\right)^{1/2}\left\langle m\mathbf{k}+\mathbf{q}\left|\delta V_{p\mathbf{q}}(\mathbf{r})\right|n\mathbf{k}\right\rangle. \quad \textbf{[S3]}$$

Here $n\mathbf{k}$ and $m\mathbf{k}+\mathbf{q}$ denote the Bloch states, and m_0 is a convenient reference mass. $\delta V_{p\mathbf{q}}$ is the perturbation of self-consistent potential induced by a phonon at state $p\mathbf{q}$, which is usually called the "phonon perturbation." The right-hand sides of Eqs. **S1** and **S2** are related to the linewidth (imaginary part of self-energy, $\Sigma_{n\mathbf{k}}^{''}$) of a particle involved in the *e*-ph interactions. The linewidth determines the time that the system can persist in its original state. For example, when an electron is added into a system, the probability amplitude of the system at state $n\mathbf{k}$ will exponentially decay by the factor of $\Sigma_{n\mathbf{k}}^{''}(\Delta t)/\hbar$ after a time period Δt (2). Therefore, one can evaluate the average lifetime for the electron in terms of the imaginary part of the self-energy by $\tau_{n\mathbf{k}}^{e\text{-ph}}=\hbar/2|\Sigma_{n\mathbf{k}}^{''}|$ and do the same for the phonon lifetime.

The phonon scattering rate due to the ph-ph interaction is given by (1)

$$\frac{1}{\tau_{p\mathbf{q}}^{\text{ph-ph}}}=\frac{\hbar\pi}{4}\sum_{p',p''}\int\frac{dq'}{\Omega_{\mathrm{BZ}}}\left[\begin{array}{c}\left|\mathbf{V}_{p\mathbf{q},+p'q'}^{p''q''}\right|^2\left(n_{+p'q'}-n_{p''q''}\right)\delta\left(\hbar\omega_{p\mathbf{q}}-\hbar\omega_{p''q''}+\hbar\omega_{+p'q'}\right)\\+\frac{1}{2}\left|\mathbf{V}_{p\mathbf{q},-p'q'}^{p''q''}\right|^2\left(n_{-p'q'}+n_{p''q''}+1\right)\delta\left(\hbar\omega_{p\mathbf{q}}-\hbar\omega_{p''q''}-\hbar\omega_{-p'q'}\right)\end{array}\right], \quad \textbf{[S4]}$$

where $\mathbf{V}_{p\mathbf{q},+p'q'}^{p''q''}$ and $\mathbf{V}_{p\mathbf{q},-p'q'}^{p''q''}$ are the coupling matrices for three-phonon processes satisfying the momentum conservation relation of $\mathbf{q}\pm q'=q''+\mathbf{G}$. Here $\mathbf{G}$ represents an arbitrary reciprocal lattice vector and, when $\mathbf{G}\neq 0$, is called the umklapp process; otherwise, it is the normal process. The first term in the brackets in Eq. **S4** is the transition possibility of the process that two phonons merge to create another phonon and the second term is vice versa. Harmonic vibrations will not generate resistance to heat flow, and therefore the ph-ph interaction arising from lattice anharmonicity acts as the major source to scatter phonons. In this point of view, the matrix element of ph-ph coupling can be evaluated by (1)

$$\mathbf{V}_{p\mathbf{q},\pm p'q'}^{p''q''}=\sum_{i,j,k}\sum_{\alpha,\beta,\gamma}\Psi_{ijk}^{\alpha\beta\gamma}\frac{\xi_{i,p\mathbf{q}}^{\alpha}\xi_{j,\pm p'q'}^{\beta}\xi_{k,p''q''}^{\gamma}}{\sqrt{m_im_jm_k\omega_{p\mathbf{q}}\omega_{\pm p'q'}\omega_{p''q''}}}, \quad \textbf{[S5]}$$

where $\Psi_{ijk}^{\alpha\beta\gamma}$ is the tensor of the third-order force constant that describes the strength of the anharmonic term in the strain-energy response. The indexes i, j, and k loop over atomic sites in the unit cell, and α, β, and γ represent the directions in Cartesian coordinates. m_i is the atomic mass, and $\xi_{i,p\mathbf{q}}^{\alpha}$ is the normalized phonon eigenmode which can be obtained by solving the dynamical matrix. In this study, the ph-*e* and ph-ph interactions are taken into account, as given by Eqs. **S2** and **S4**, respectively, to calculate the phonon scattering rate. A convenient way to evaluate the total scattering rate is by using the Matthiessen's rule, $1/\tau_{p\mathbf{q}}^{\text{tot}}=1/\tau_{p\mathbf{q}}^{\text{ph-ph}}+1/\tau_{p\mathbf{q}}^{\text{ph-}e}$, which is based on the assumption that the two scattering channels are independent of each other.

In this work, we neglect the scatterings arising from impurity; however, the doping effect is characterized by the position of the Fermi level, which can be calculated by a given carrier concentration and temperature. Once the electron and phonon scattering rates are obtained, the electron transport properties can be calculated according to the Onsager reciprocal relations: $S=L_{12}/L_{11}$, $\sigma=-L_{11}$, and $\kappa_e=L_{11}-L_{21}L_{12}/L_{11}$, where the coefficients are given by (3)

$$L_{11} = -\frac{g_e e^2}{\Omega N_{\mathbf{k}}} \sum_{n\mathbf{k}} v_{n\mathbf{k}}^{\alpha} v_{n\mathbf{k}}^{\beta} \tau_{n\mathbf{k}}^{e\text{-ph}} \frac{\partial f_{n\mathbf{k}}}{\partial \varepsilon_{n\mathbf{k}}}, \quad \textbf{[S6]}$$

$$L_{12} = \frac{g_e e}{\Omega N_{\mathbf{k}} T} \sum_{n\mathbf{k}} (\varepsilon_{n\mathbf{k}} - \varepsilon_f) v_{n\mathbf{k}}^{\alpha} v_{n\mathbf{k}}^{\beta} \tau_{n\mathbf{k}}^{e\text{-ph}} \frac{\partial f_{n\mathbf{k}}}{\partial \varepsilon_{n\mathbf{k}}}, \quad \textbf{[S7]}$$

$$L_{21} = \frac{g_e e}{\Omega N_{\mathbf{k}}} \sum_{n\mathbf{k}} (\varepsilon_{n\mathbf{k}} - \varepsilon_f) v_{n\mathbf{k}}^{\alpha} v_{n\mathbf{k}}^{\beta} \tau_{n\mathbf{k}}^{e\text{-ph}} \frac{\partial f_{n\mathbf{k}}}{\partial \varepsilon_{n\mathbf{k}}}, \quad \textbf{[S8]}$$

and

$$L_{22} = -\frac{g_e}{\Omega N_{\mathbf{k}} T} \sum_{n\mathbf{k}} (\varepsilon_{n\mathbf{k}} - \varepsilon_f)^2 v_{n\mathbf{k}}^{\alpha} v_{n\mathbf{k}}^{\beta} \tau_{n\mathbf{k}}^{e\text{-ph}} \frac{\partial f_{n\mathbf{k}}}{\partial \varepsilon_{n\mathbf{k}}}. \quad \textbf{[S9]}$$

Here ε_f is the Fermi energy, $v_{n\mathbf{k}}^{\alpha}$ is the electron group velocity, and $N_{\mathbf{k}}$ is the number of sampled $\mathbf{k}$-point grids in the Brillouin zone. The lattice thermal conductivity can be calculated by (3)

$$\kappa_{\text{ph}} = \frac{1}{\Omega N_{\mathbf{q}}} \sum_{p\mathbf{q}} \hbar \omega_{p\mathbf{q}} v_{p\mathbf{q}}^{\alpha} v_{p\mathbf{q}}^{\beta} \tau_{p\mathbf{q}}^{\text{tot}} \frac{\partial n_{p\mathbf{q}}}{\partial T}, \quad \textbf{[S10]}$$

where $v_{p\mathbf{q}}^{\alpha}$ is the phonon group velocity, and $N_{\mathbf{q}}$ is the number of sampled $\mathbf{q}$-point grids. Based on the RTA, the electron and phonon MFPs are calculated by $\lambda_{n\mathbf{k}}^{e} = |\mathbf{v}_{n\mathbf{k}}| \tau_{n\mathbf{k}}^{e\text{-ph}}$ and $\lambda_{p\mathbf{q}}^{\text{ph}} = |\mathbf{v}_{p\mathbf{q}}| \tau_{p\mathbf{q}}^{\text{tot}}$, respectively. Note that the electron and phonon properties are tensors with dimensions $\alpha \times \beta$; the scalar transport properties can be obtained by averaging the diagonal elements since the electron and phonon transports are isotropic in SnTe.

Simulation Details. To obtain the coupling matrices of the *e*-ph and ph-ph interactions as shown by Eqs. **S3** and **S5**, the electronic Hamiltonian, phonon perturbation, and interatomic force constants should be determined in the first place. In this work, these quantities are computed by using the Quantum ESPRESSO package (4). A fully relativistic norm-conserving pseudopotential with Becke–Perdew parameterization of exchange-correlation functional including generalized gradient approximation (GGA) is employed to calculate the electronic Hamiltonian and phonon perturbation, while a fully relativistic norm-conserving pseudopotential with Perdew–Zunger parameterization of exchange-correlation functional including local density approximation (LDA) is employed to calculate the second- and third-order interatomic force constants. We use the different pseudopotentials to treat the electron and phonon parts, because the GGA functional can characterize the V-shape band structure as well as give a better band offset between the first and second valence bands. On the other hand, the LDA functional can provide a more accurate optimized lattice constant and thus avoid imaginary phonon frequency particularly near the Brillouin zone center. A $16 \times 16 \times 16$ and a $6 \times 6 \times 6$ Monkhorst–Pack $\mathbf{k}$-point mesh are employed in the self-consistent and nonself-consistent field calculations, respectively. The cutoff energy of the plane wave is 70 Ry, and the convergence threshold for energy is set to be 10^{-12} Ry for both pseudopotentials. In the density-functional perturbation theory (DFPT) calculation, a $6 \times 6 \times 6$ $\mathbf{q}$-point mesh is employed to compute the dynamical matrices (second-order force constant can be obtained through its Fourier transform) and phonon perturbations. The threshold for DFPT calculation is chosen as 10^{-21} Ry to achieve the better convergence especially to the phonon perturbation. For the calculation of third-order force constant, a $4 \times 4 \times 4$ supercell associated with a $2 \times 2 \times 2$ $\mathbf{k}$-point mesh is used to compute the atomic stresses. The cutoff distance of the force constant is 6 Å to improve the computational efficiency.

Once these quantities are obtained, in this study, the EPW (5) and ShengBTE (6) packages are employed to compute the coupling matrices and the self-energies of *e*-ph and ph-ph interactions, respectively. Our in-house code, an iterative solver of the linearized BTE integrated with the EPW and ShengBTE packages, is developed to compute the thermoelectric properties and their MFP spectrum. The *e*-ph scattering rates are computed on a $200 \times 200 \times 200$ $\mathbf{k}$-point mesh associated with a $100 \times 100 \times 100$ $\mathbf{q}$-point mesh, and the ph-*e* scattering rates are computed on a $30 \times 30 \times 30$ $\mathbf{q}$-point mesh associated with a $60 \times 60 \times 60$ $\mathbf{k}$-point mesh. The computation of ph-ph scattering rate is performed on a $30 \times 30 \times 30$ $\mathbf{q}$-point mesh. With these fine-mesh ab initio scattering rates, the thermoelectric properties and MFP spectrum can be calculated by Eqs. **S6**–**S10**.

Comparisons for ab Initio Results with Experiments. Here, we provide the discussion on the discrepancies in the crystal structure and transport properties between the pristine and stoichiometric SnTe.

Cell parameter and electronic band structure. The optimized cell parameter from our ab initio calculation is 6.209 Å, which is close to the experimental measurement (6.327 Å) on a SnTe sample with 1.5% Sn vacancies. The calculated energy gap is about 0.09 eV, and we have expanded it to match the experimental bandgap, 0.18 eV (7)—a rigid band approximation. The underestimation of cell parameter and the bandgap is commonly expected as a result of the inherent approximation in the exchange-correlation functional used in ab initio calculation (8). Furthermore, a first-principles study (9) has shown that the effect of Sn vacancy on the valence band is only a slight increase of the electron density of states. These discrepancies in crystal structure and band dispersion are not significant, and therefore the rigid band approximation is justified in our calculations.

Mobility and Seebeck coefficient. The ab initio mobilities of the pristine SnTe (Fig. S1*D*) show good agreement with the experimental measurements in the low-carrier concentration regime. The deviation can be found when the sample is heavily doped, which could result from the electron ionized-impurity interactions that are not taken into account in the calculation. For the Seebeck coefficient, the positions of local minimum and maximum take place at lower carrier concentrations compared with experiments. This is because

the energy offset between the first and second valence bands from our ab initio calculation (0.25 eV, Fig. S1*A*) is slightly smaller than the suggested value (0.31 eV) fitted from experimental Seebeck coefficients (7, 10).

Lattice and electronic thermal conductivities. Previous experimental studies report room-temperature lattice and electronic thermal conductivities of 2.0~3.1 W/mK and 5.0~6.3 W/mK, respectively, at carrier concentrations between 1.0×10^{20} cm^{-3} and 4.5×10^{20} cm^{-3} (10–14). Our simulation results of lattice and electronic thermal conductivities are about 5.3 W/mK and 8.0 W/mK, respectively, in reasonable agreement with the experimental values. The discrepancy can be attributed to the existence of Sn vacancies, which leads to defect scatterings.

Model for Studying Electron MFP Filtering. When the change of lattice constant is small, and the crystal potential in the strained lattice depends only on the local displacement, the perturbed potential due to lattice vibration can be expressed as $U = \mathbf{M}_{p\mathbf{q}} u_{p\mathbf{q}}$, where $u_{p\mathbf{q}}$ is the Fourier component of the phonon at mode p and wavevector $\mathbf{q}$, and $\mathbf{M}_{p\mathbf{q}}$ is the coupling matrix of the e-ph interaction. The piezoelectric interaction will not occur in SnTe due to the existence of inversion symmetry (15). The e-ph coupling matrices of acoustic-deformation potential, optical-deformation potential and polar-optical-phonon interactions are, respectively, given by (16)

$$|\mathbf{M}^{\mathrm{ADP}}_{p\mathbf{q}}|^2 = D^2_{\mathrm{ADP}} q^2, \qquad \text{[S11]}$$

$$|\mathbf{M}^{\mathrm{ODP}}_{p\mathbf{q}}|^2 = D^2_{\mathrm{ODP}}, \qquad \text{[S12]}$$

and

$$|\mathbf{M}^{\mathrm{POP}}_{p\mathbf{q}}|^2 = \frac{\rho e^2 \omega^2_{p\mathbf{q}}}{q^2 \epsilon_0} \left(\epsilon_\infty^{-1} - \epsilon_s^{-1}\right). \qquad \text{[S13]}$$

Here D_{ADP} and D_{ODP} are the deformation potentials of acoustic and optical phonons, respectively. $\omega_{p\mathbf{q}}$ is the phonon frequency, ρ is the mass density, and ϵ_0 is the vacuum permittivity. The e-ph scattering rate is the key factor in evaluating electron transport properties in semiconductors and insulators. Based on Fermi's golden rule, the scattering rate of the electron at band n and wavevector $\mathbf{k}$ is given by (16)

$$\frac{1}{\tau^{e\text{-ph}}_{n\mathbf{k}}} = \frac{2\pi}{\hbar} \sum_{m\mathbf{k}\pm\mathbf{q}, p\mathbf{q}} |\mathbf{M}_{p\mathbf{q}}|^2 \frac{\hbar\left(n_{p\mathbf{q}} + \frac{1}{2} \mp \frac{1}{2}\right)}{2\rho\Omega\omega_{p\mathbf{q}}} \delta_{n\mathbf{k}, m\mathbf{k}\pm\mathbf{q}} \delta\left(\varepsilon_{m\mathbf{k}+\mathbf{q}} - \varepsilon_{n\mathbf{k}} \mp \hbar\omega_{p\mathbf{q}}\right). \qquad \text{[S14]}$$

Here $\varepsilon_{n\mathbf{k}}$ is the electron energy, and Ω is the volume of the unit cell. The Debye model is employed to describe the dispersion relation of acoustic phonons, while optical phonons are assumed to be dispersionless. In this work, we investigate the electron MFP filtering effect in the two types of electronic band structures: the Dirac band and the nonparabolic Kane band, of which the dispersion relations are given by $\varepsilon = \pm\sqrt{m^2 + \Sigma_i v^2_{f,i} k^2_i}$ and $\varepsilon(1 + \delta\varepsilon) = \hbar^2|\mathbf{k}|^2/2m_{eff}$, respectively. The obtained scattering rate will be used to estimate the ratio of the optimal power factor, $\sigma_{opt}S^2_{opt}/\sigma_{bulk}S^2_{bulk}$, by solving the Boltzmann transport equation (*Carriers' Interactions and Transport Properties*), where $\sigma_{opt}S^2_{opt}$ is the highest power factor given by an optimal cutoff of electron MFP λ_{opt} in the spectrum. For example, in Fig. 3*B* (main text), $\lambda_{opt} \sim 20$ nm is obtained when the carrier concentration is 1.0×10^{20} cm^3. The results of enhancement of the power factor are shown in Fig. S5.

With this model, we can study the effect of band shape and dielectric screening on the enhancement of power factor by varying the band nonparabolicity δ, Fermi velocity v_f, and factor of strength of phonon-induced dipole $\epsilon_\infty^{-1} - \epsilon_s^{-1}$. A smaller $\epsilon_\infty^{-1} - \epsilon_s^{-1}$ is relevant to weaker polar-optical-phonon interaction basically due to stronger dielectric screening. The parameters used in this work are given as follows. For the Dirac band model, the Fermi velocities are $v_{f,1} = v_{f,2} = 3.5 \times 10^5$ and $v_{f,3} = 5.5 \times 10^5$ m/s in transverse and longitudinal directions, respectively, and the Dirac mass m is set to be 0.09 eV. For the Kane band model, the effective masses of electron are $0.15m_0$ and $0.06m_0$ in transverse and longitudinal directions, respectively. The phonon group velocities of transverse- and longitudinal-acoustic modes are 1,500 and 3,000 m/s, respectively, and the phonon frequencies at the Brillouin zone center of transverse- and longitudinal-optical modes are 4.0 THz and 5.0 THz, respectively. For the e-ph coupling matrices, the deformation potentials of acoustic and optical phonons are $D_{\mathrm{ADP}} = 10.0$ eV and $D_{\mathrm{ODP}} = 2.0$ eV/Å, respectively.

1. Ziman JM (1960) *Electrons, and Phonons: The Theory of Transport Phenomena in Solids* (Oxford Univ Press, New York).
2. Giustino F (2017) Electron-phonon interactions from first principles. *Rev Mod Phys* 89:015003.
3. Chen G (2005) *Nanoscale Energy Transport and Conversion: A Parallel Treatment of Electrons, Molecules, Phonons, and Photons* (Oxford Univ Press, New York).
4. Giannozzi P, et al. (2009) QUANTUM ESPRESSO: A modular and open-source software project for quantum simulations of materials. *J Phys Condens Matter* 21:395502.
5. Poncé S, Margine ER, Verdi C, Giustino F (2016) EPW: Electron-phonon coupling, transport and superconducting properties using maximally localized Wannier functions. *Comput Phys Commun* 209:116–133.
6. Li W, Carrete J, Katcho NA, Mingo N (2014) ShengBTE: A solver of the Boltzmann transport equation for phonons. *Comput Phys Commun* 185:1747–1758.
7. Rogers LM (1968) Valence band structure of SnTe. *J Phys D Appl Phys* 1:845–852.
8. Martin RM (2008) *Electronic Structure: Basic Theory and Practical Methods* (Cambridge Univ Press, Cambridge, UK).
9. Tan XJ, et al. (2016) Element-selective resonant state in M-doped SnTe (M = Ga, In, and Tl). *Phys Chem Chem Phys* 18:20635–20639.
10. Zhou M, et al. (2014) Optimization of thermoelectric efficiency in SnTe: The case for the light band. *Phys Chem Chem Phys* 16:20741–20748.
11. Tan G, et al. (2014) High thermoelectric performance of *p*-type SnTe via a synergistic band engineering and nanostructuring approach. *J Am Chem Soc* 136:7006–7017.
12. Zhang Q, et al. (2013) High thermoelectric performance by resonant dopant indium in nanostructured SnTe. *Proc Natl Acad Sci USA* 110:13261–13266.
13. Tan G, et al. (2015) Codoping in SnTe: Enhancement of thermoelectric performance through synergy of resonance levels and band convergence. *J Am Chem Soc* 137:5100–5112.
14. Banik A, Vishal B, Perumal S, Datta R, Biswas K (2016) The origin of low thermal conductivity in $Sn_{1-x}Sb_xTe$: Phonon scattering via layered intergrowth nanostructures. *Energy Environ Sci* 9:2011–2019.
15. Hsieh TH, et al. (2012) Topological crystalline insulators in the SnTe material class. *Nat Commun* 3:982.
16. Lundstrom M (2009) *Fundamentals of Carrier Transport* (Cambridge Univ Press, Cambridge, UK).

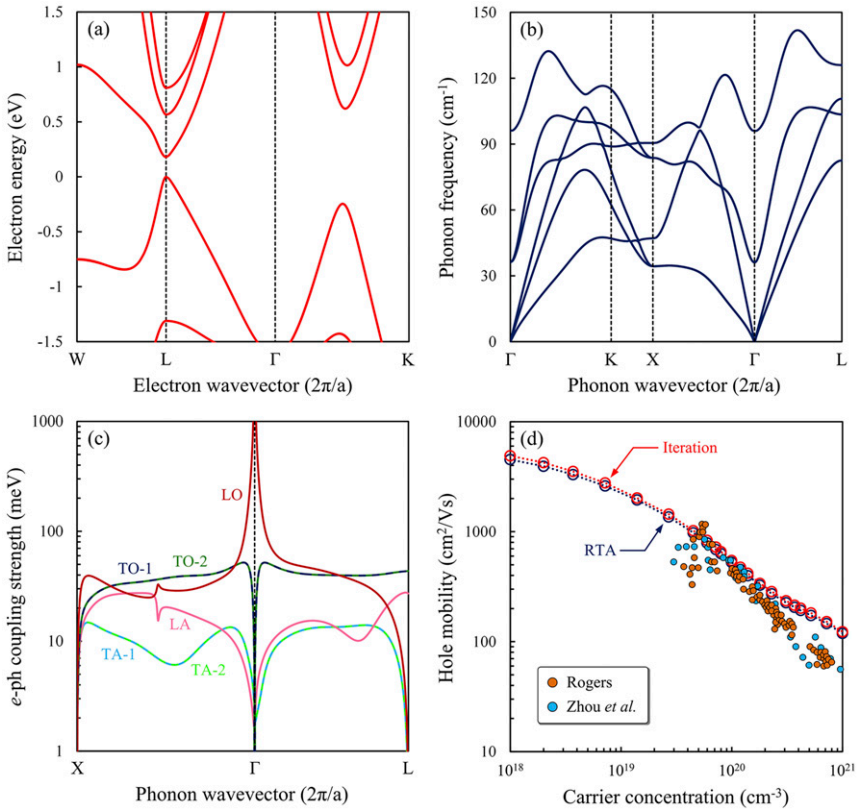

Fig. S1. Calculated material properties of SnTe. (*A*) Electron band structure of SnTe. The band structure is calculated by using a pseudopotential with a GGA-BP functional. The energy offset between the first and second valence bands is 0.25 eV. The band gap has been expanded to 0.18 eV, using a rigid band model. (*B*) Phonon band structure of SnTe. The dispersion relation is calculated by using a pseudopotential with an LDA-PZ functional. The optimized lattice constant is 6.209 Å. (*C*) The *e*-ph coupling strength ($|\mathbf{M}_{nk,p\mathbf{q}}^{mk+\mathbf{q}}|$) of SnTe. It indicates the strength of an electron at the L point (valence band edge) coupling with phonons along two high-symmetry lines from Γ to X points and Γ to L points. The divergent behavior ($\sim|\mathbf{q}|^{-1}$) of the LO mode near the Γ point is due to the induced long-range dipole field, exhibiting the importance of considering polar-optical-phonon interaction in constructing the *e*-ph matrix. (*D*) Ab initio hole mobility of SnTe at 300 K with different *p*-type carrier concentrations. The blue and red circles are, respectively, computed by RTA and the exact solution solving from linearized BTE using an iterative scheme (1). We found that the iterative procedure will not affect the mobility too much, which averages about 7% within the studied range of carrier concentration. The computational results are in agreement with the experimental measurements (7, 10) except for very high carrier concentration. This difference mainly comes from the impurity scattering due to the existence of defects and vacancies, which are introduced in heavily doped material in experiments.

1. Liu TH, Zhou J, Liao B, Singh DJ, Chen G (2017) First-principles mode-by-mode analysis for electron-phonon scattering channels and mean free path spectra in GaAs. *Phys Rev B* 95:075206.

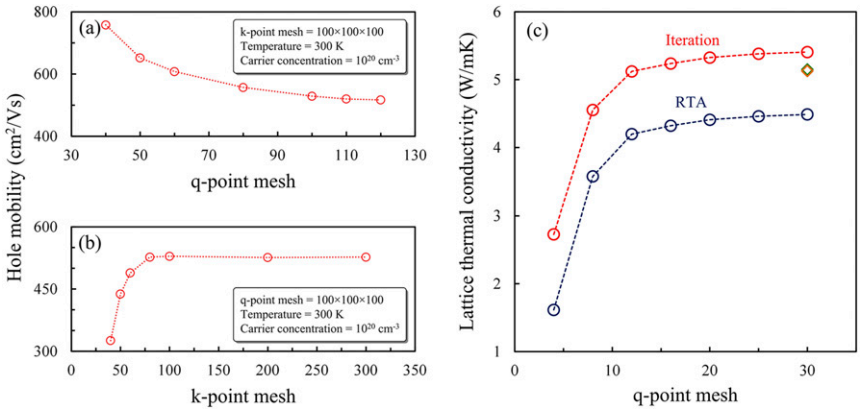

Fig. S2. Convergence tests for hole mobility and lattice thermal conductivity of SnTe. (*A* and *B*) Convergence tests with respect to varying (*A*) **q**-point mesh and (*B*) **k**-point mesh. We found that a 200 × 200 × 200 **k**-point mesh associated with a 100 × 100 × 100 **q**-point mesh achieves the best balance between mobility convergence and computational efficiency and is employed to compute electron transport properties throughout this work. (*C*) Convergence test for thermal conductivity of SnTe with respect to varying **q**-point mesh. We found that a 30 × 30 × 30 **q**-point mesh is sufficient to achieve converged lattice thermal conductivity. The exact solution solving from linearized BTE is used to obtain more accurate lattice thermal conductivity since it has about 20% variation during the iterations. The green and orange diamonds are the lattice thermal conductivities with consideration of ph-e scattering rates calculated by a 60 × 60 × 60 **k**-point mesh and a 30 × 30 × 30 **k**-point mesh, respectively.

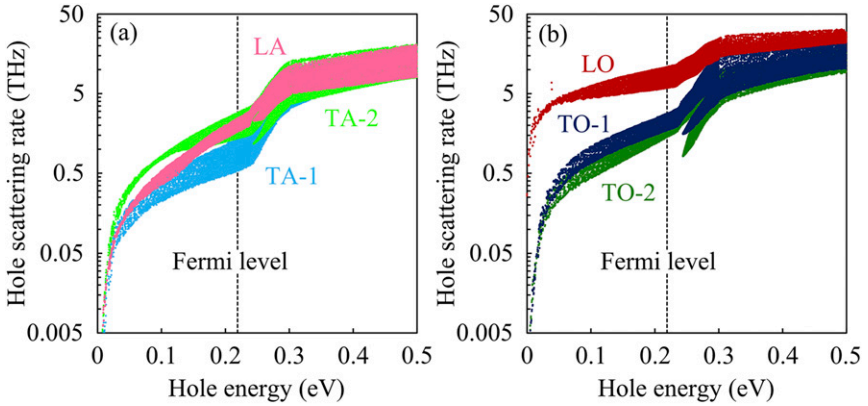

Fig. S3. Hole scattering rates arising from each phonon mode. (*A*) Energy-dependent hole scattering rates due to each acoustic mode. (*B*) Energy-dependent hole scattering rates due to each optical mode.

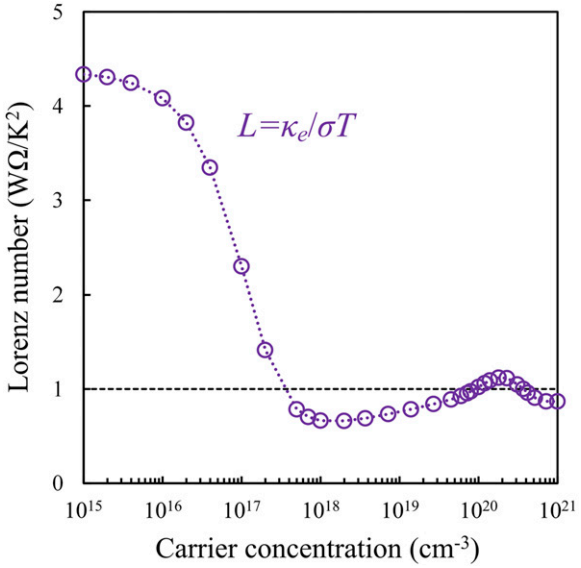

Fig. S4. Ab initio normalized Lorenz number of SnTe at 300 K with respect to different carrier concentration. The Lorenz number has been normalized to the standard value ($L_0 = 2.45 \times 10^{-8}$ WΩ/K^2). The normalized value of intrinsic SnTe is 4.34 and then rapidly approaches 0.87 as the carrier concentration increases.

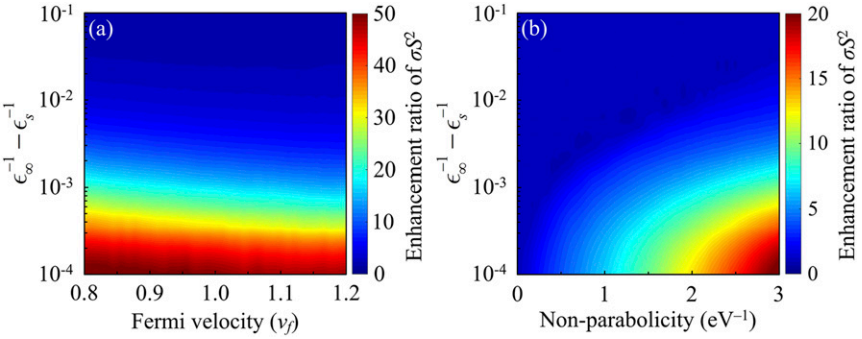

Fig. S5. Electron MFP filtering effect for different types of band structures. (*A*) Enhancement ratio of power factor of the Dirac band with varying Fermi velocity and $\epsilon_\infty^{-1}-\epsilon_s^{-1}$. The studied range is from $0.8v_f$ to $1.2v_f$. (*B*) Enhancement ratio of power factor of the nonparabolic band with varying band non-parabolicity and $\epsilon_\infty^{-1}-\epsilon_s^{-1}$. *A* and *B*, respectively, correspond to Fig. 4 *B* and *C* in the main text.

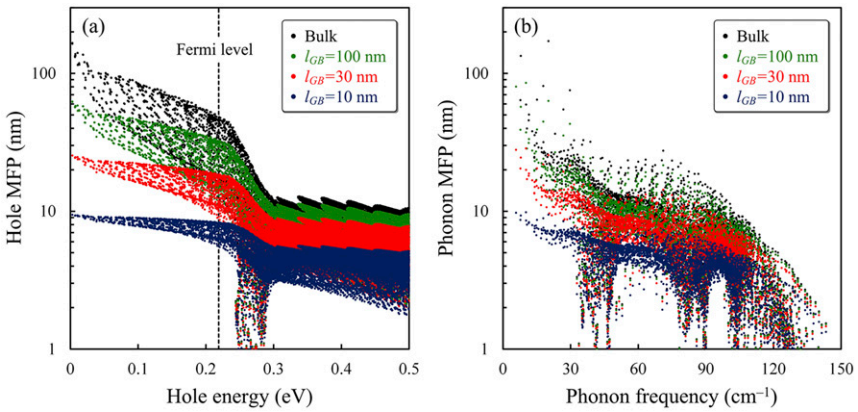

Fig. S6. Carriers' MFPs limited by boundary scattering due to different characteristic lengths. (*A* and *B*) The variation of MFPs of (*A*) holes and (*B*) phonons. The black dots represent bulk MFPs without boundary scattering. The green, red, and blue dots show the reductions of MFPs when the boundaries with characteristic lengths l_{GB} = 100 nm, 30 nm, and 10 nm are applied, respectively. The electron and phonon MFPs are calculated at 300 K and a *p*-type carrier concentration of 1.0×10^{20} cm^{-3}.